NASA/TM—2011-217025

Reynolds-Averaged Navier-Stokes Solutions to Flat Plate Film Cooling Scenarios

Perry L. Johnson
University of Central Florida, Orlando, Florida

Vikram Shyam and Chunill Hah
Glenn Research Center, Cleveland, Ohio

May 2011

NASA STI Program . . . in Profile

Since its founding, NASA has been dedicated to the advancement of aeronautics and space science. The NASA Scientific and Technical Information (STI) program plays a key part in helping NASA maintain this important role.

The NASA STI Program operates under the auspices of the Agency Chief Information Officer. It collects, organizes, provides for archiving, and disseminates NASA's STI. The NASA STI program provides access to the NASA Aeronautics and Space Database and its public interface, the NASA Technical Reports Server, thus providing one of the largest collections of aeronautical and space science STI in the world. Results are published in both non-NASA channels and by NASA in the NASA STI Report Series, which includes the following report types:

- TECHNICAL PUBLICATION. Reports of completed research or a major significant phase of research that present the results of NASA programs and include extensive data or theoretical analysis. Includes compilations of significant scientific and technical data and information deemed to be of continuing reference value. NASA counterpart of peer-reviewed formal professional papers but has less stringent limitations on manuscript length and extent of graphic presentations.

- TECHNICAL MEMORANDUM. Scientific and technical findings that are preliminary or of specialized interest, e.g., quick release reports, working papers, and bibliographies that contain minimal annotation. Does not contain extensive analysis.

- CONTRACTOR REPORT. Scientific and technical findings by NASA-sponsored contractors and grantees.

- CONFERENCE PUBLICATION. Collected papers from scientific and technical conferences, symposia, seminars, or other meetings sponsored or cosponsored by NASA.

- SPECIAL PUBLICATION. Scientific, technical, or historical information from NASA programs, projects, and missions, often concerned with subjects having substantial public interest.

- TECHNICAL TRANSLATION. English-language translations of foreign scientific and technical material pertinent to NASA's mission.

Specialized services also include creating custom thesauri, building customized databases, organizing and publishing research results.

For more information about the NASA STI program, see the following:

- Access the NASA STI program home page at *http://www.sti.nasa.gov*

- E-mail your question via the Internet to *help@sti.nasa.gov*

- Fax your question to the NASA STI Help Desk at 443–757–5803

- Telephone the NASA STI Help Desk at 443–757–5802

- Write to:
  NASA Center for AeroSpace Information (CASI)
  7115 Standard Drive
  Hanover, MD 21076–1320

Reynolds-Averaged Navier-Stokes Solutions to Flat Plate Film Cooling Scenarios

Perry L. Johnson
University of Central Florida, Orlando, Florida

Vikram Shyam and Chunill Hah
Glenn Research Center, Cleveland, Ohio

National Aeronautics and
Space Administration

Glenn Research Center
Cleveland, Ohio 44135

May 2011

Acknowledgments

Level of Review: This material has been technically reviewed by technical management.

Available from

NASA Center for Aerospace Information
7115 Standard Drive
Hanover, MD 21076–1320

National Technical Information Service
5301 Shawnee Road
Alexandria, VA 22312

Available electronically at http://www.sti.nasa.gov

Reynolds-Averaged Navier-Stokes Solutions to Flat Plate Film Cooling Scenarios

Perry L. Johnson
University of Central Florida
Orlando, Florida 32816

Vikram Shyam and Chunill Hah
National Aeronautics and Space Administration
Glenn Research Center
Cleveland, Ohio 44135

Abstract

The predictions of several Reynolds-Averaged Navier-Stokes solutions for a baseline film cooling geometry are analyzed and compared with experimental data. The Fluent finite volume code was used to perform the computations with the realizable k-ε turbulence model. The film hole was angled at 35° to the crossflow with a Reynolds number of 17,400. Multiple length-to-diameter ratios (1.75 and 3.5) as well as momentum flux ratios (0.125 and 0.5) were simulated with various domains, boundary conditions, and grid refinements. The coolant to mainstream density ratio was maintained at 2.0 for all scenarios. Computational domain and boundary condition variations show the ability to reduce the computational cost as compared to previous studies. A number of grid refinement and coarsening variations are compared for further insights into the reduction of computational cost. Liberal refinement in the near hole region is valuable, especially for higher momentum jets that tend to lift-off and create a recirculating flow. A lack of proper refinement in the near hole region can severely diminish the accuracy of the solution, even in the far region. The effects of momentum ratio and hole length-to-diameter ratio are also discussed.

Nomenclature

D coolant hole nominal diameter, measured at the inlet to the hole, [m]

DR density ratio, ρ_c / ρ_∞

I momentum flux ratio, $\left(\rho U^2\right)_c \big/ \left(\rho U^2\right)_\infty$

k thermal conductivity, [W/mK]

L coolant pipe length, [m]

M mass flux ratio, $\left(\rho U\right)_c \big/ \left(\rho U\right)_\infty$

p pitch (distance between two neighboring coolant holes), [m]

P_0 operating pressure, [kPa]

R gas constant for air, [287 J/kg*K]

T temperature, [K]

U mean velocity, [m/s]

U^* dimensionless mean velocity

x distance downstream (from the centerline of coolant outlet), [m]

y vertical distance (from the hole exit and adiabatic surface), [m]

z lateral distance (from the centerline of the coolant outlet), [m]

Greek symbols:

α angle of hole-axis inclination [°]

η local adiabatic film cooling effectiveness

$\bar{\eta}$ laterally-averaged adiabatic film cooling effectiveness

$\bar{\bar{\eta}}$ spatially-averaged adiabatic film cooling effectiveness

θ dimensionless temperature, as in Reference 11

θ^* dimensionless temperature

ρ density [kg/m^3]

Subscripts:

aw   adiabatic wall

c   coolant

CL   centerline

r   recovery

∞ crossflow freestream

Introduction

Gas turbine engines, used not only for aero-propulsion but also for land-based electrical power generation, operate at higher efficiencies when the firing temperature is increased. Modern engines operate well in excess of the allowable temperatures of metal components in the early turbine stages downstream of the combustion chamber. To compensate, "coolant" air is bled from the compressor, through internal passages, cooling the turbine components before injection into the hot gas path through discrete angled film cooling holes. After injection the coolant ideally provides a blanket (or "film") of cooler air on the surface of the components, thus shielding them from the damaging temperatures of the hot gas path. As the use of compressor air lowers the performance of the engine, the goal of film cooling is to achieve a careful design balance which requires thorough knowledge of the physics involved in the interactions of the injected coolant and the hot crossflow.

Film cooling is evaluated primarily by its adiabatic effectiveness, Equation (1), on the downstream surface. It is common to compare effectiveness trends along the line directly downstream of the center of the hole exit, Equation (2). An alternative measurement is the span-wise averaged effectiveness, Equation (3), which accounts for the effectiveness on the entire downstream surface.

$$\eta(x,z) = \frac{T_r - T_{aw}(x,z)}{T_r - T_{c,\text{exit}}} \tag{1}$$

$$\eta_{CL}(x) = \eta(x,0) \tag{2}$$

$$\bar{\eta}(x) = \frac{\int \eta(x,z)\,dz}{\int dz} \tag{3}$$

In the research laboratory, an easy film cooling model is the use of a flat plate geometry downstream of scaled cylindrical holes. Even with this basic geometry, a number of factors can influence the effectiveness of the film cooling. Due to large temperature differences, a large density gradient between the coolant jet and hot crossflow is present, as quantitatively specified by a density ratio (*DR*), Equation (4). Multiplication of the density ratio by a velocity magnitude ratio (*VR*), Equation (5), the blowing ratio, or mass-flux ratio (*M*) is obtained, Equation (6). A fourth parameter is the momentum-flux (*I*) ratio, Equation (7). Two of these four influential hydrodynamic parameters are independent.

$$DR = \frac{\rho_c}{\rho_\infty} \tag{4}$$

$$VR = \frac{U_c}{U_\infty} \tag{5}$$

$$M = \frac{(\rho U)_c}{(\rho U)_\infty} \tag{6}$$

$$I = \frac{\left(\rho U^2\right)_c}{\left(\rho U^2\right)_\infty} \tag{7}$$

While the *VR* affects whether the crossflow perceives the injected jet as a blockage or an acceleration, *M* and *I* have greater success in scaling the results across multiple *DR*. For example, *I* usually determines closely the trajectory of the jet as it exits the cooling hole (Refs. 1 and 2). Three different regimes for film cooling can be defined for simple angle cylindrical holes. First, at low momentum ratios ($I < 0.3$-0.4), the coolant jet is deflected immediately toward the wall, providing maximum coverage to the centerline downstream of the hole. Once the momentum ratio is increased (0.3-$0.4 < I < 0.7$-0.8), the jet slightly detaches from the downstream surface and penetrates into the crossflow before reattaching further downstream. Higher momentum flux ratios ($I > 0.7$-0.8) results in complete lift-off of the jet and minimal film cooling effectiveness downstream. This analysis is based on the experiments of Sinha et al. (Ref. 1) and Thole et al. (Ref. 2) at an inclination angle (α) of 35°.

Geometric parameters can also have great influence on the film cooling flow. The inclination angle of a cooling hole is the most obvious geometric parameter. The present study is concerned only with the simplest of film cooling hole shapes: a row of stream-wise cylindrical holes. The cylindrical hole was naturally the first discrete hole shape studied. Goldstein et al. studied a single cylindrical hole (Ref. 3) and a row of cylindrical holes (Ref. 4), reporting adiabatic wall effectiveness. Eriksen and Goldstein (Ref. 5) studied the heat transfer behind such a row of holes. Goldstein et al. (Ref. 6) began to look at geometric and hydrodynamic effects, specifically density ratio and hole length.

Pedersen et al. (Ref. 7) studied the effect of density ratio in more detail using the heat-mass transfer analogy, as did Foster and Lampard (Ref. 8) in their study of cylindrical holes. Pietrzyk et al. (Refs. 9 and 10) studied the velocity field of the film cooling situation at density ratios of 1.0 and 2.0, considering both mean and statistical turbulent data. Sinha et al. (Ref. 1) extended the density ratio study to provide adiabatic effectiveness results. Thole et al. (Ref. 2) continued further with mean thermal field measurements. As previously mentioned, these two studies bench-marked the trajectory regimes of cylindrical film cooling flows. Since the coolant is usually supplied to the hole from a large plenum-like area, the exit velocity profile is not fully-developed. Consequently, the length-to-diameter ratio is an important parameter when the length of the hole fails to exceed about 5 diameters (Refs. 11 and 12).

Walters and Leylek (Ref. 13) provided a robust methodology for RANS simulations of film cooling flows. Using the standard *k*-ε turbulence model with a gradient adapted unstructured grid and two-layer wall treatment, they compared against the surface data of Sinha et al. (Ref. 1). Azzi and Lakehal (Ref. 14) and Lakehal (Ref. 15) made anisotropic and turbulent Reynolds number corrections to the *k*-ε equations, showing improvement in the centerline effectiveness predictions of the experiments of (Ref. 1). Recently, Large Eddy Simulations (LES), as opposed to RANS, has grown in the field of film cooling research (Refs. 16 to 22). RANS, however, remains the workhorse for practical engineering applications due to the relative computational ease as compared to LES. In either circumstance, computational domain, boundary conditions, and grid resolution are important balances of computational efficiency and solution accuracy.

The present study investigates the domain, boundary, and resolution considerations using a RANS approach in the context of the *L/D* and *I* comparisons available in the experimental work of (Refs. 1 and 2). RANS then can be made a stepping stone to the computationally rigorous LES method, where such considerations become even more important.

Approach

Grid resolution, as in any numerical simulation, is key to the proper computational solution of film cooling. Overly coarse grids will lead to gross inaccuracies in the solution while overly fine grids will waste time and computational resources. In regions with high gradients in flow properties, finer grids are needed to properly resolve the flow, whereas, more uniform regions can be accurately represented by a coarser grid. The design of a grid should incorporate the minimum number of cells while still accurately capturing the physics of the flow field. This current study investigated a number of different grid structures in evaluating the ability of RANS approaches to predict film cooling flows.

Because film cooling from cylindrical holes tends to exhibit a large range of jet trajectories, the current study was designed to look at how this may affect the ability of the current RANS approach to predict film cooling effectiveness. The highest momentum ratios, with complete detachment, are generally avoided in film cooling design. Therefore, the current study simulated two momentum flux ratios at an engine-like density ratio of 2.0. The low momentum ratio, with expected full attachment, was 0.125, mirroring the experiments of Sinha et al. (Ref. 1) and Thole et al. (Ref. 2). The moderate momentum ratio, $I = 0.5$, also matched experiments from the same investigations. These two studies were performed at different length-to-diameter ratios, thus, the current study also needed to reflect this. Sinha et al. used very short holes with L/D = 1.75, while Thole et al. studied longer holes with L/D = 3.5. With these two variables (momentum-flux and length-to-diameter ratios), a total of four cases were defined for the current study. Table 1 summarizes the test matrix. Table 2 gives the common parameters for all studies.

TABLE 1.—TEST MATRIX

Scope of investigation	$I = 0.125$	$I = 0.5$
L/D = 1.75 (Sinha et al.)	Case 1	Case 2
L/D = 3.5 (Thole et al.)	Case 3	Case 4

TABLE 2.—GEOMETRY AND FLOW CONDITIONS

D	12.7 mm
α	35°
p/D	3.0
U_∞	20 m/s
$Tu\%_\infty$	0.2%
T_∞	300 K
T_c	150 K
DR	2.0
M	0.5, 1.0
δ_{99}/D	0.52

Within each of these four cases, a variety of different grids were tested. First, a basic grid with a thin layer of wall refinement was used as a baseline to test boundary condition effects. Type 'a-c' grids fell into this category, of which the grid structure near the hole is shown in Figure 1(a). Type 'c' grids used the full computational domain of Walters and Leylek (Ref. 13). Type 'b' grids shortened the modeled crossflow by a factor of two while type 'a' grids went a step further and shortened the modeled crossflow inlet length, replacing its effects with a 1/7 law boundary layer profile (Refs. 14, 15, and 19), Equation (8), with experimentally specified boundary layer thickness. In all, this led to a 40 percent reduction in grid cells.

$$U(y) = U_\infty \left(\frac{y}{\delta} \right)^{\frac{1}{7}} \tag{8}$$

Next, the grid was highly refined in the region near the hole, with regions away from the hole generally unaffected. This new refinement gave rise to grids 'd' and 'f', Figure 1(b). The 'f' grids encompassed the entire domain of (Ref. 13) while the 'd' grids represented the full domain reduction similar to 'a' grids. Following the near-hole refinement in 'd' and 'f' grids, a coarsening was applied to the entire flow field to generate grid 'i', Figure 1(c). This coarsening was an attempt to generate similarly accurate solutions as grid 'd', but with greatly reduced computation time. Finally, the jet region, as defined by the upper 0.5 diameters of the plenum, the coolant hole, and the lower two diameters above the crossflow surface, was refined using hanging node adaption. The result of this final grid refinement was labeled 'j', Figure 1(d). In hanging node adaption, parent hexahedral cells are split into four children
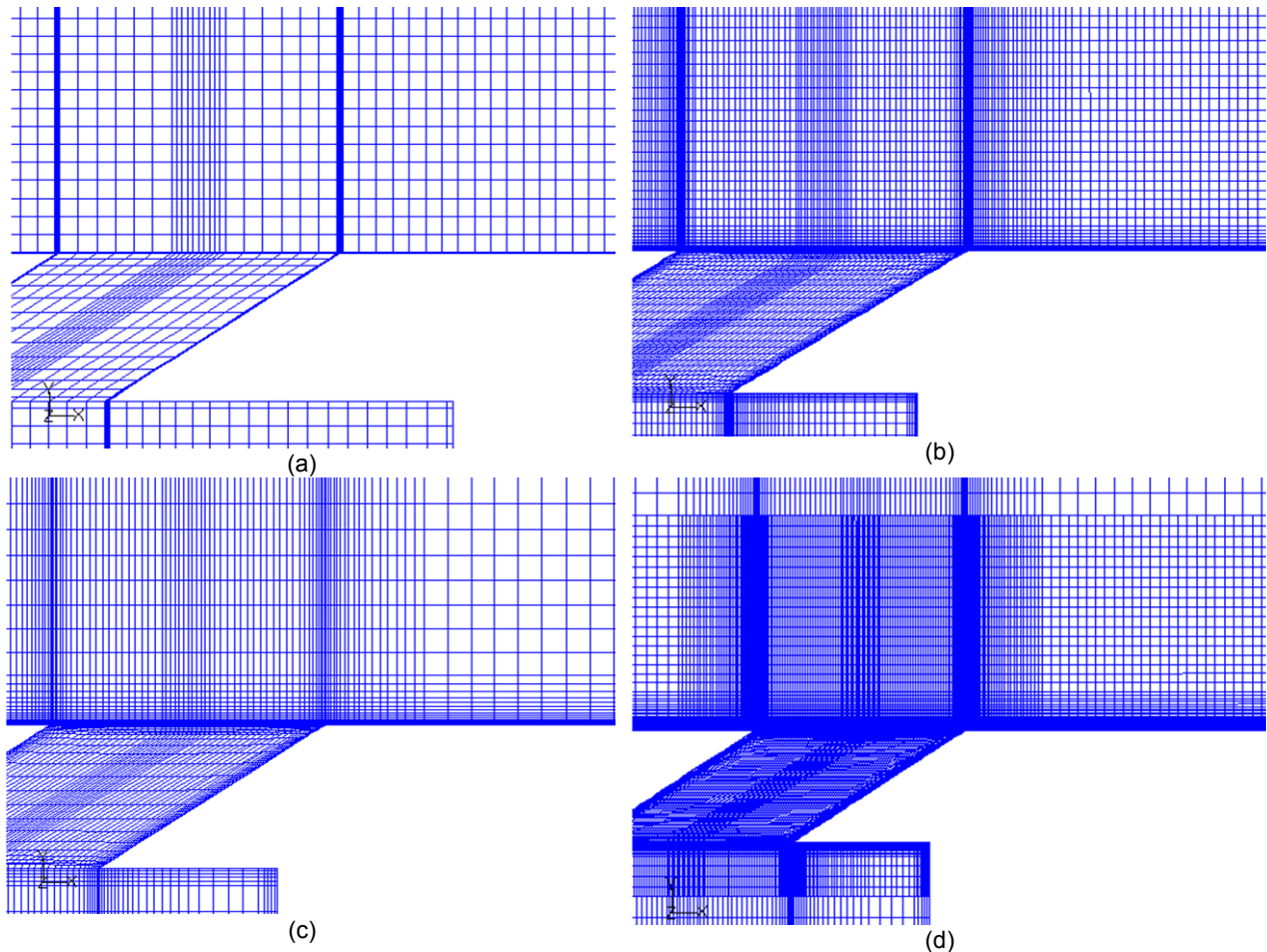

(a)

(b)

(c)

(d)

Figure 1.—Grid topologies used: (a) initial spacing ('a', 'b', and 'c'), (b) with near-hole refinement ('d' and 'f'), (c) with subsequent total coarsening ('i') and (d) with hanging node adaption in the jet region ('j').

hexahedral cells. If the adaption is preformed only for a portion of the grid, the boundary of the adapted and non-adapted regions gives rise to hanging nodes, which results from a parent face's connection with four children faces. Extra memory overhead is needed to maintain connectivity, but effective use can significantly reduce cell count and computation time. A two-dimensional schematic of a hanging node is shown in Figure 2.

To appreciate the domain reductions involved in changing from the Walters and Leylek grids 'c' and 'f' to grids 'a' and 'd', the domains are shown side by side in Figure 3 with identical plenum and hole sizes. In all, this reduction led to about a grid with about 40 percent of the cells of the full domain.

Not all cases were run for each grid. Table 3 summarizes the entire spectrum of numerical simulations performed in the current study. With four cases and seven grid structures, a total of 19 simulations were completed. These solutions enabled comparisons with respect to momentum-flux ratio, length-to-diameter ratio, and grid refinement/coarsening.
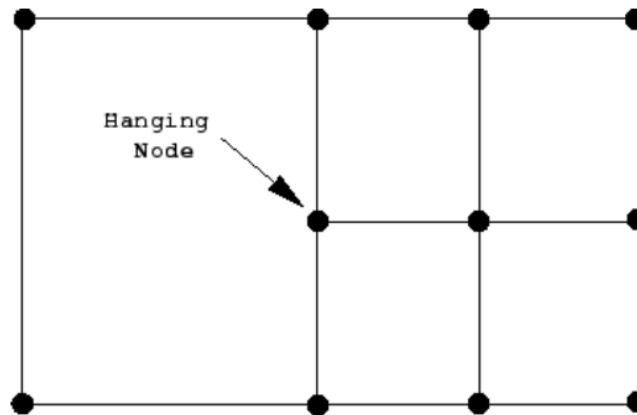
Figure 2.—Schematic of a hanging node resulting from the hexahedral adaption process (Ref. 23).
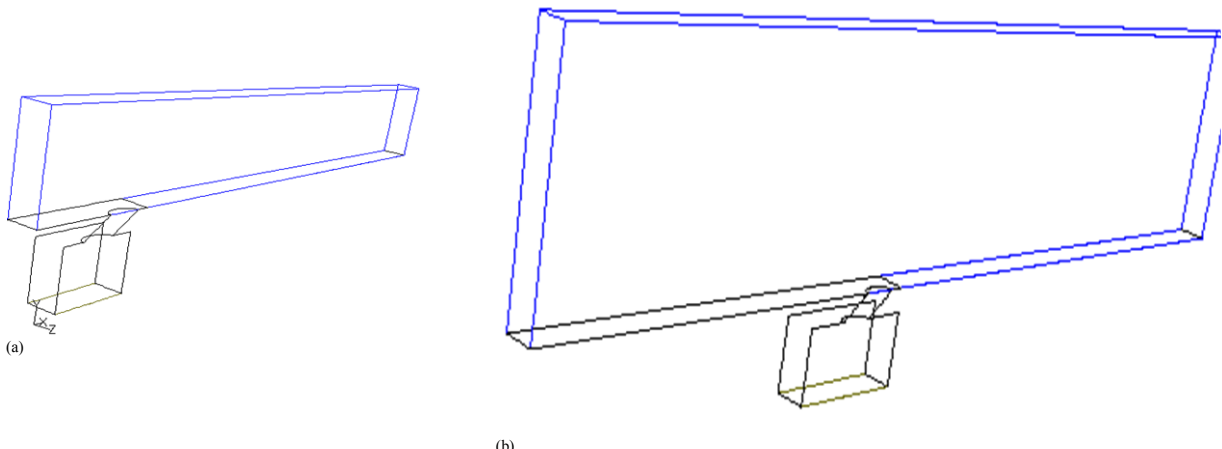
Figure 3.—Computational domains: (a) reduced grids 'a','d','i','j' and (b) full grids 'c','f'.

TABLE 3.—LIST OF GRIDS USED FOR EACH CASE

Grid letter	Description	Cell count in millions	Cases used
a	Fully reduced domain	0.21	1,2,3,4
b	Partially reduced domain	0.29	1,2
c	Full domain of (Ref. 13)	0.50	1,2,3,4
d	Grid 'a' with near hole refinement	0.77	1,2,3,4
f	Grid 'c' with near hole refinement	1.31	1,2
i	Grid 'd' with universal coarsening	0.19	1,2
j	Grid 'i' with hanging node adaption in jet region	1.03	2

Numerical Methodology

The numerical domain was established to mirror the experiments of Sinha et al. and Thole et al., the important difference between the two experiments being the length of the hole. Some of the grids represented the domain used by Walters and Leylek (Ref. 13), which stretched ten diameters above the no-slip surface and 20 diameters upstream of the hole. The fully-reduced domain modeled only five diameters above the surface and five diameters upstream of the holes. Because a row of holes was being modeled, only one-half of the hole needed to be modeled for the steady solution.

The plenum and crossflow walls were specified with adiabatic no-slip conditions, while symmetry planes in the span-wise direction were specified with zero shear and zero heat-flux. The "freestream" condition was approximated using a symmetry boundary as well. The plenum and crossflow inlets were specified by a velocity profile. The near-stagnation plenum was always supplied with a uniform inlet velocity profile while the crossflow was given a uniform profile for the long upstream length cases ('b','c','f') and a 1/7 law velocity profile (Eq. (8)) for the reduced upstream length cases ('a','d','i','j'). A pressure-outlet condition controlled the pressure (101.325 kPa) at the crossflow outlet, though the absolute pressure was unimportant for the incompressible solution.

Gambit (Ref. 23) grid generation software was used for all grids. The structured hexahedral grids, though varying for each case, maintained overall the same structure, with certain refinement or coarsening in certain areas. All cases, to varying degrees, maintained refinement near no-slip walls, placing the first node with a y+ on the order of unity.

Fluent's (Ref. 24) pressure-based incompressible solver with energy equation was used to solve the governing equations with the specified boundary conditions. The governing equations were solved in the Reynolds-Averaged Navier-Stokes form with the realizable k-ε turbulence model to achieve closure. Though modeled as incompressible with respect to pressure, the ideal-gas relation was used with nominal pressure to relate density to temperature, Equation (9). This relationship allowed for the creating of a density ratio of 2.0 as previously discussed.

$$\rho = \frac{P_0}{RT} \qquad (9)$$

Near the walls, Fluent's enhanced wall treatment (two-layer model) was used for improved accuracy over standard wall-functions. Discretization was accomplished with a second-order upwind scheme for the convective terms and central differencing scheme for the diffusive terms. The SIMPLE segregated algorithm was used to deal with pressure/velocity coupling. For a given iteration, the three momentum (velocity) equations were solved sequentially, followed by a pressure-correction continuity equation. After the fluxes were updated based on these new solutions, scalar values such as temperature and turbulence quantities were updated. Convergence was dictated by three criteria: scaled residuals below 10^{-6}, iterative convergence of local surface temperature monitors, and global conservation errors for mass and energy more than three orders of magnitude below the overall mass and energy flows. The aggression of the solution convergence process was dictated by relaxation factors for each of the equations. These relaxation parameters were started low to avoid divergence, then increased as the solution began successfully converging toward lower scaled residuals. For detail on the above techniques, the reader is referred to the Fluent User's Guide.

Results and Discussion

Validation With Previous Studies: Grid Effects

Each of the four cases are first compared against their respective experimental results from Sinha et al. (Ref. 1) or Thole et al. (Ref. 2). Case 1 was the low momentum ratio for the short holes in Reference 1. Figure 4 compares the experimental results of centerline effectiveness with the various numerical solutions from the current investigation. The results from the unstructured, adaptive grid of Walters and Leylek (Ref. 13) as well as the structured grid of Azzi and Lakehal (Ref. 14) are shown alongside the present results. In general the present results over-predict the centerline effectiveness, as would be expected based on previous knowledge of the turbulent anisotropy of the film cooling flow. Cases 'a', 'b', and 'c' produced effectiveness values identical to one another, indicating that the domain reductions had no effect on the surface conditions predicted by the solver. Grids 'd' and 'f', however, slightly deviate from the first three with slightly lower effectiveness near the hole but slightly higher effectiveness 5 to 15 diameters downstream. Other grid coarsening and refinement still failed to closely predict the experimental results, as one might expect given the assumptions of the turbulence models.

Figure 5 presents the span-wise averaged effectiveness trends with downstream distance for the same case. Numerical solutions here show under-prediction of the effectiveness, further reinforcing the under-prediction of the lateral spreading as the cause for over prediction of centerline effectiveness.

The under-prediction of lateral spreading is clearly shown in Figure 6, where effectiveness is shown in the spanwise direction. Over-prediction of effectiveness at the centerline is balanced by under-prediction of effectiveness at the mid-span. The overall effect, referring back to Figure 5, is a slight under-prediction of laterally-averaged effectiveness.
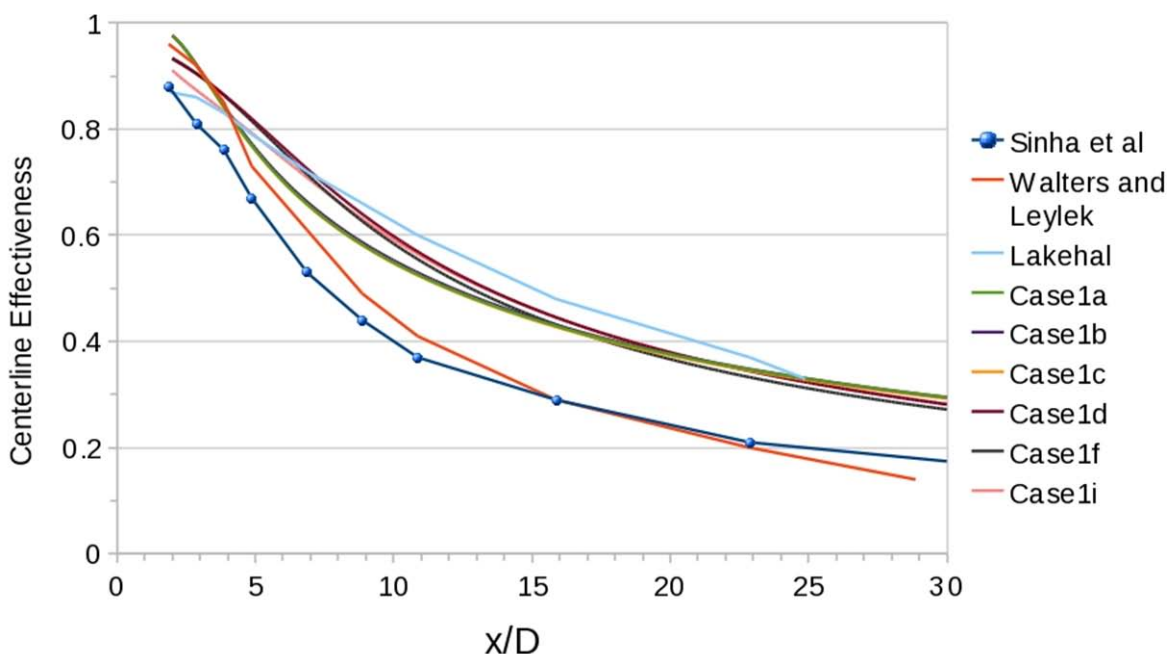

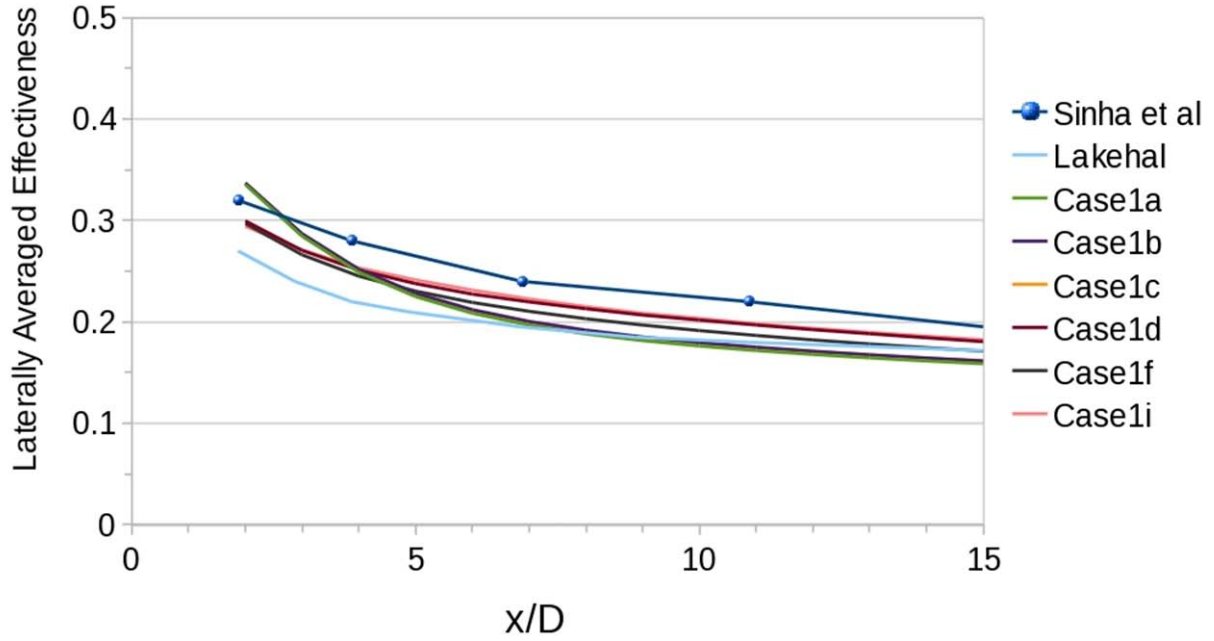Figure 4.—Centerline effectiveness for Case 1: *L/D* = 1.75, *I* = 0.125.

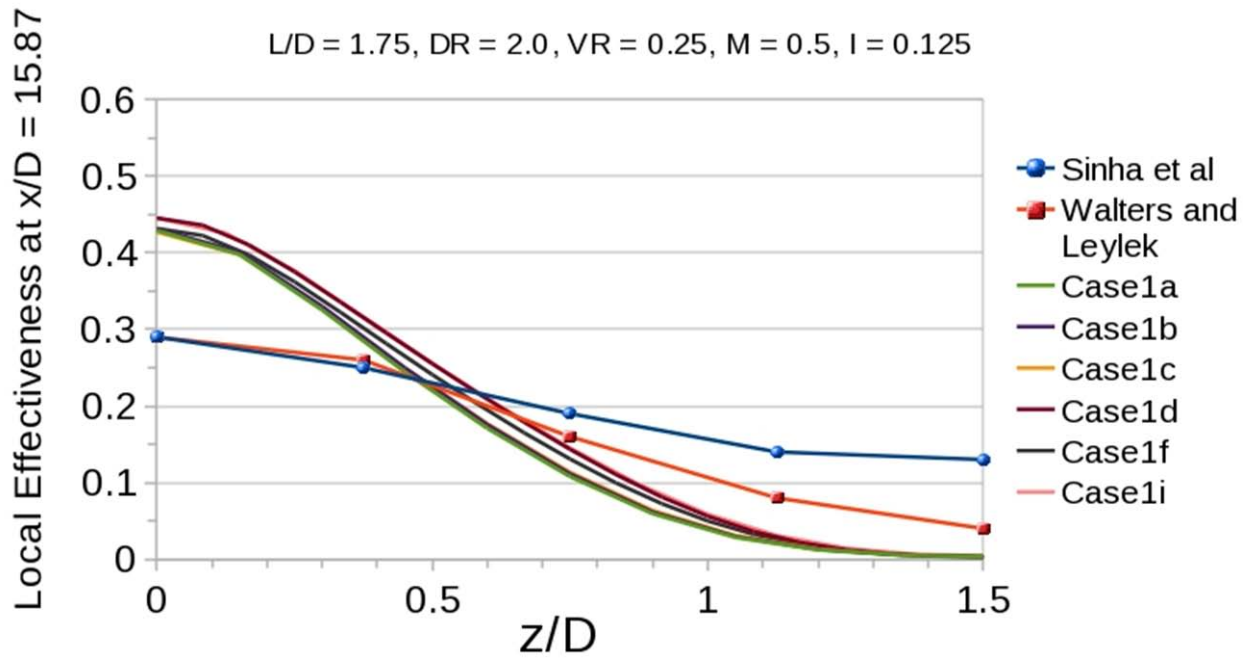Figure 5.—Laterally-averaged effectiveness for Case 1: *L/D* = 1.75, *I* = 0.125.

Figure 6.—Local effectiveness in the span-wise direction for Case 1: *L/D* = 1.75, *I* = 0.125.

Case 2 results are compared in Figures 7 to 9 against the higher momentum ratio ($I = 0.5$) from (Ref. 1). The experimental centerline results in Figure 7 suggest a lift-off and reattachment regime, yielding far lower effectiveness values near the hole. The 'a', 'b', and 'c' grids (again, agreeing with one another) fail to predict any sort of jet lift-off. The grid refinement in the near-hole region (grids 'd' and 'f') do capture the jet lift-off region. The lift-off is still captured, even with the coarsening of grid 'i' down to under 200,000 cells. The failure to predict the near hole lift-off (grids 'a', 'b', 'c') is detrimental to the rest of the prediction downstream. The correct prediction, however, does not need great resolution in the main body of flow, just in the region near the exit lip of the hole. There is still an overall over-prediction of centerline effectiveness for the refined numerical solutions, indicating the under-prediction of lateral spreading still applies at the higher momentum ratio. The original grids ('a', 'b', and 'c') show an under-prediction of centerline effectiveness at most x/D. The trends suggest that the separation of the jet is delayed by a coarse grid in the region of the jet exit. This exaggerates the effect of the lift-off and fails to capture a noticeable reattachment. Therefore, the coarseness in the region of the hole exit throws off the rest of the solution downstream.
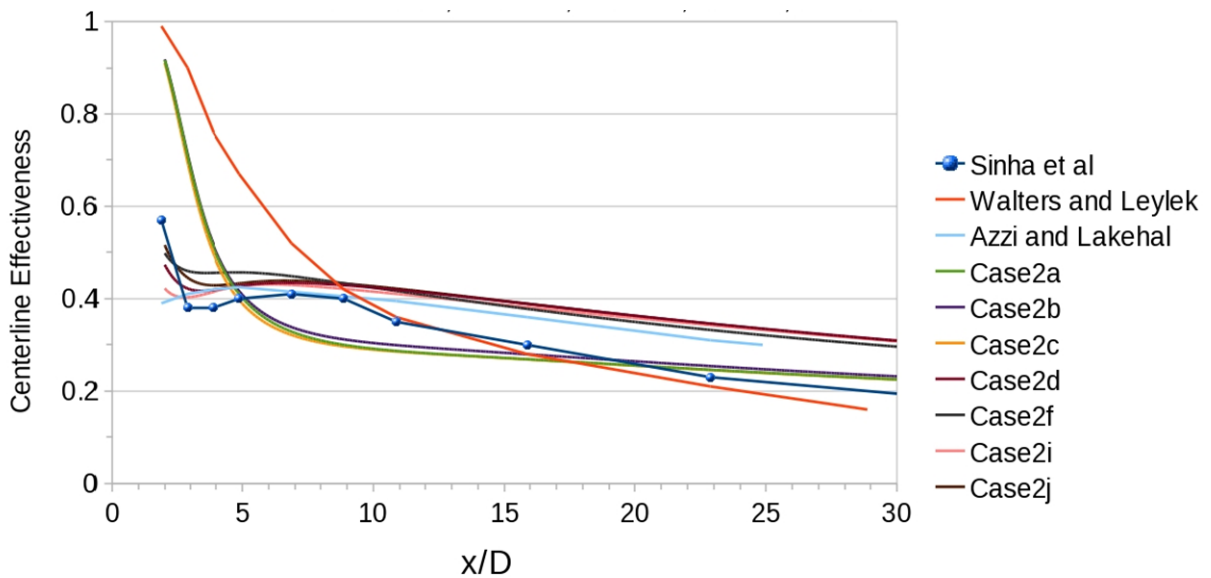

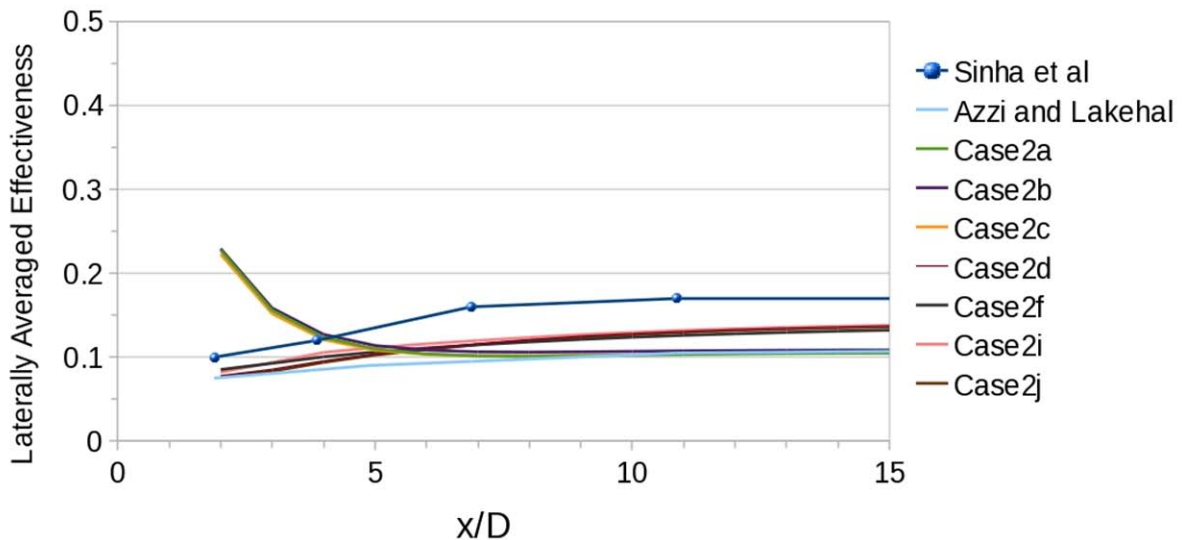Figure 7.—Centerline effectiveness for Case 2: $L/D = 1.75$, $I = 0.5$.

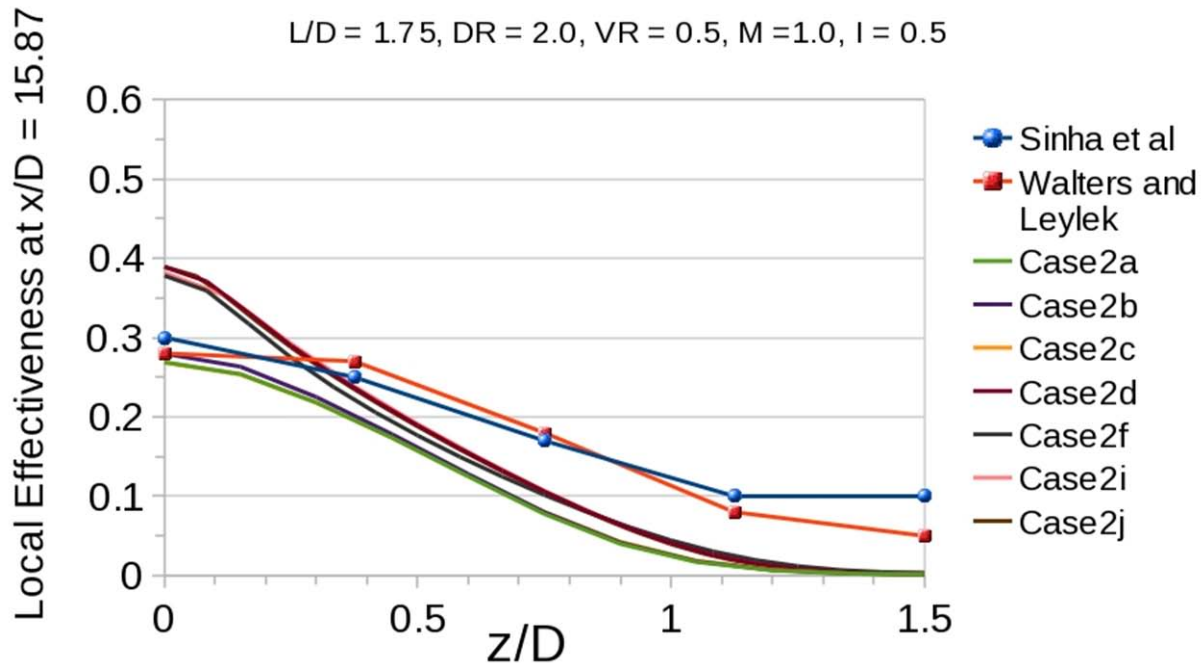Figure 8.—Laterally averaged effectiveness for Case 2: $L/D = 1.75$, $I = 0.5$.

Figure 9.—Local effectiveness in the span-wise direction for Case 2: *L/D* = 1.75, *I* = 0.5.

Case 2 laterally averaged results in Figure 8 again show an under-prediction compared to the experiments, reiterating the lack of lateral spreading. The trend of the effectiveness with *x/D* is matched much closer by the refined grids. The near hole resolution greatly effects the solution at all *x/D*. Again, the general coarsening in grid 'i' confirms that the extra refinement needed in near the hole can be balanced by a coarser mainstream, yielding similar solutions with significant reduction in computational cells.

Figure 9 compares lateral spreading predictions from the current simulations with the experimental data from Sinha et al. Again, there is obvious lack of lateral spreading. The higher effectiveness at the centerline is balanced by lower effectiveness near the mid-span. As in the case with the lower momentum ratio, the net result is slight under-prediction of laterally-averaged results. In general, the current simulations are able to capture the trends of effectiveness values fairly accurately, though the quantitative values may not be correct.

Cases 3 and 4 correspond to the temperature field measurements of Thole et al. (Ref. 2). For Case 3 validation, temperature profiles in the wall normal direction are compared at three different downstream distances in Figure 10. Near the hole, a slight over-prediction of jet trajectory seems to be apparent in the profiles. The refined grid at the hole exit captures the shape of the profiles much more closely than the original grids.

Case 4, with higher momentum ratio, provides a better chance for comparison. Figure 11 shows the temperature profiles in the wall normal direction for the same *x/D* locations as above. It is clear from these profiles that the under-prediction seen in Case 2 effectiveness plots is due to a significant over-prediction of the jet trajectory. This is not a feature of the turbulence model, however, as the refinement in the near hole region corrects the disagreement and leads to much closer agreement in effectiveness and jet trajectory. Figure 12 presents the contours of temperature throughout the flow. Here, the trajectory differences are quite clear. Even the refined grid projects a slightly higher trajectory than the experimental results, but this could be attributable to the turbulence model. Still, as in all previous results, it is worth reiterating that, trajectory aside, the jet core temperature is over-predicted, perhaps as a consequence of the turbulent model assumption of isotropic eddy diffusivity or constant turbulent Prandtl number (Ref. 15).
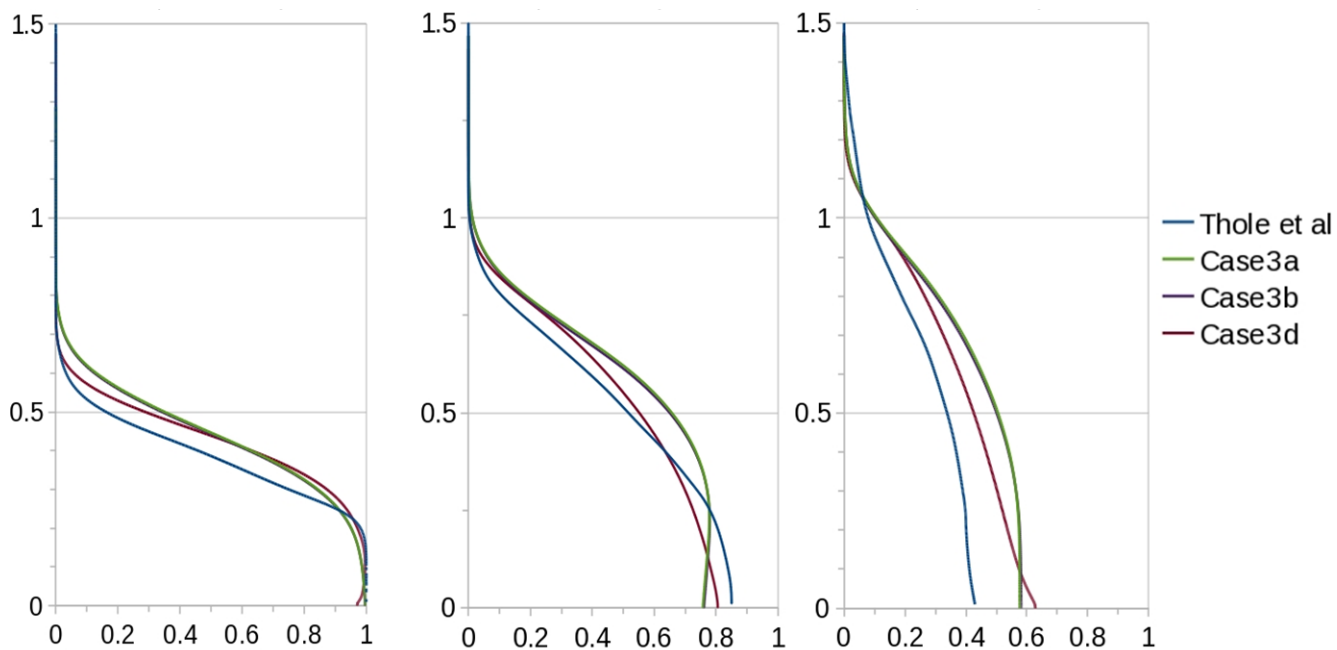
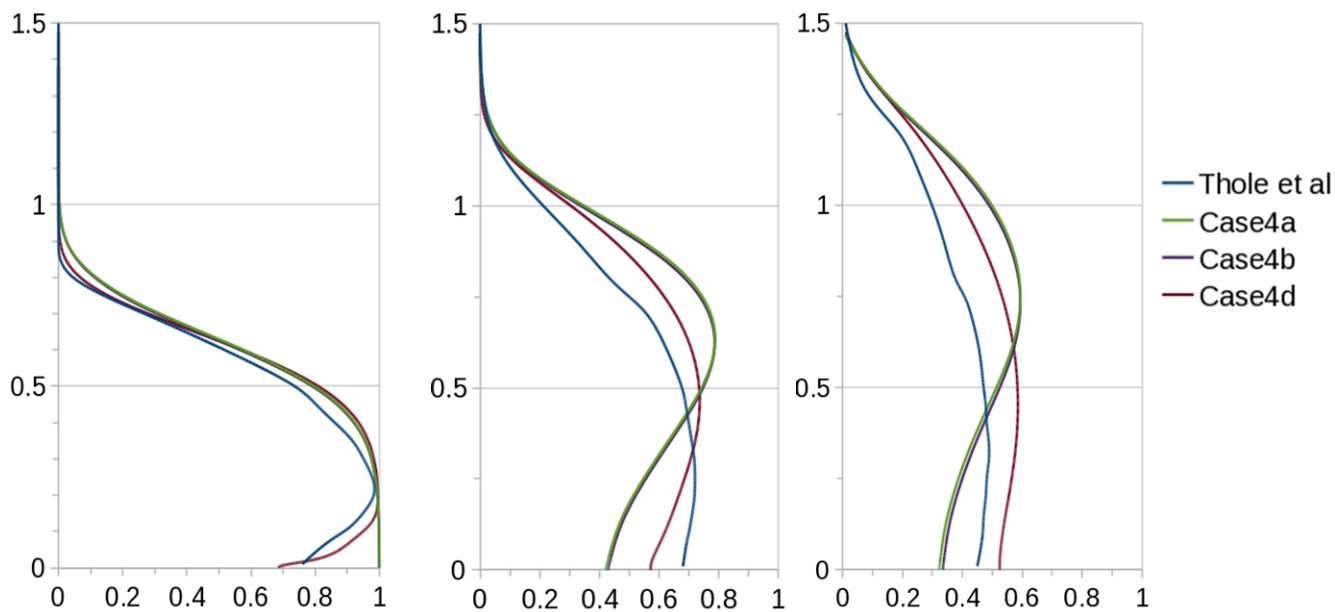Figure 10.—Wall normal nondimensional temperature profiles for Case 3: *L/D* = 3.5, *I* = 0.125.

Figure 11.—Wall normal nondimensional temperature profiles for Case 4: *L/D* = 3.5, *I* = 0.5.
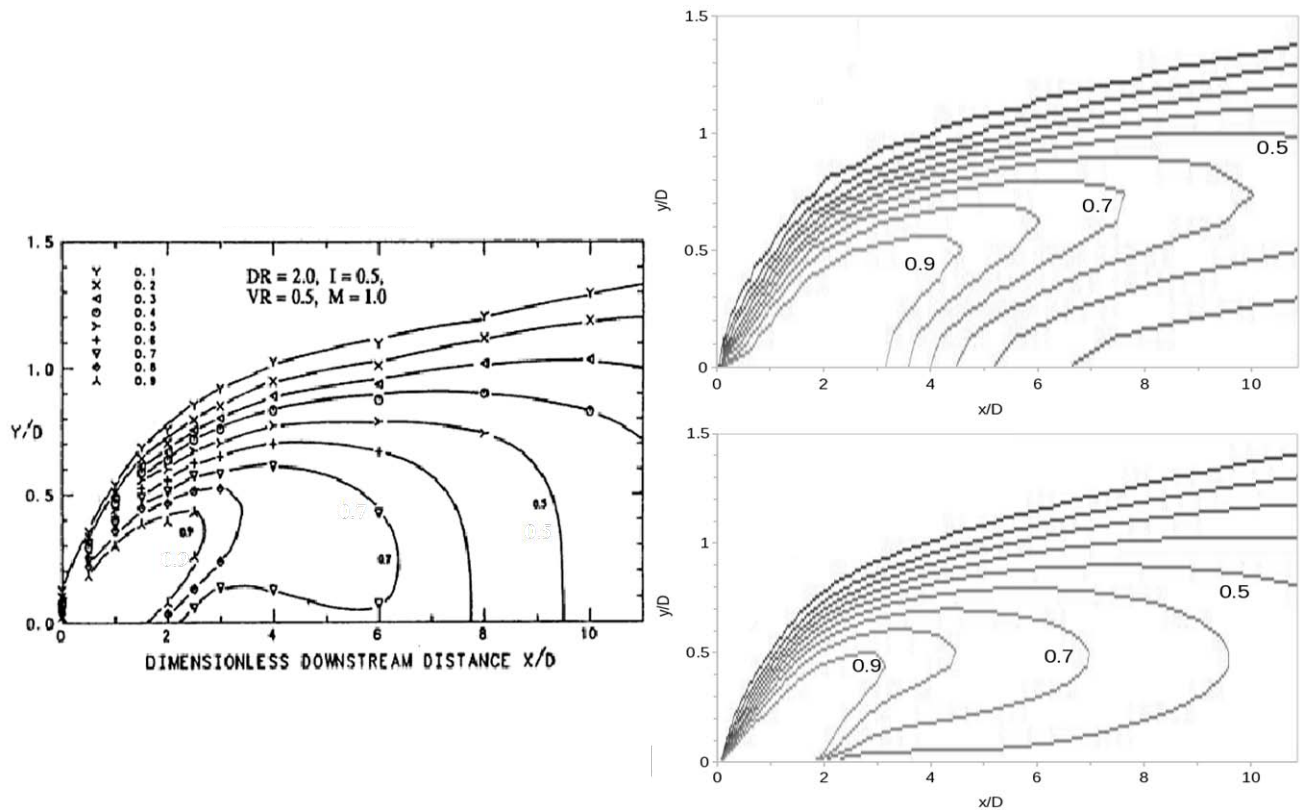
Figure 12.—Center-plane non-dimensional temperature contours for Case 4: *L/D* = 3.5, *I* = 0.5.

Momentum Ratio Effects

For the remainder of the paper, grid 'd' results will be used to compare between cases, as this grid yielded the best results and most accurately reflects the behavior of the turbulence model. Figure 13 compares centerline effectiveness results for Cases 1 and 2, corresponding to the shorter length holes with two different momentum ratios. It is obvious that the lift-off occurring in the higher momentum ratio yields a much lower effectiveness in the near hole region. Upon reattachment, however, the higher momentum jet approaches and overtakes the low momentum jet in effectiveness around $x/D = 15$ in the experiment and $x/D = 23$ in the numerical solution. In the far field, the higher momentum ratio yields slightly better effectiveness, despite near hole lift-off, as shown by both experimental and numerical evidence. The common theme is over-prediction of centerline results.

The corresponding laterally averaged results for Cases 1 and 2 are compared in Figure 14. Here, the low momentum jet gives rise to a monotonically decreasing effectiveness, as in the centerline. The higher momentum jet, however, appears to monotonically increase in effectiveness within the first 15 diameters. It is clearly flattening out, however, and if the results were extended further, would be shown to decrease. Again, it appears as though, despite beginning much lower near the hole, the effectiveness of the high momentum jet is overtaking the low momentum jet somewhere downstream of 15 diameters.
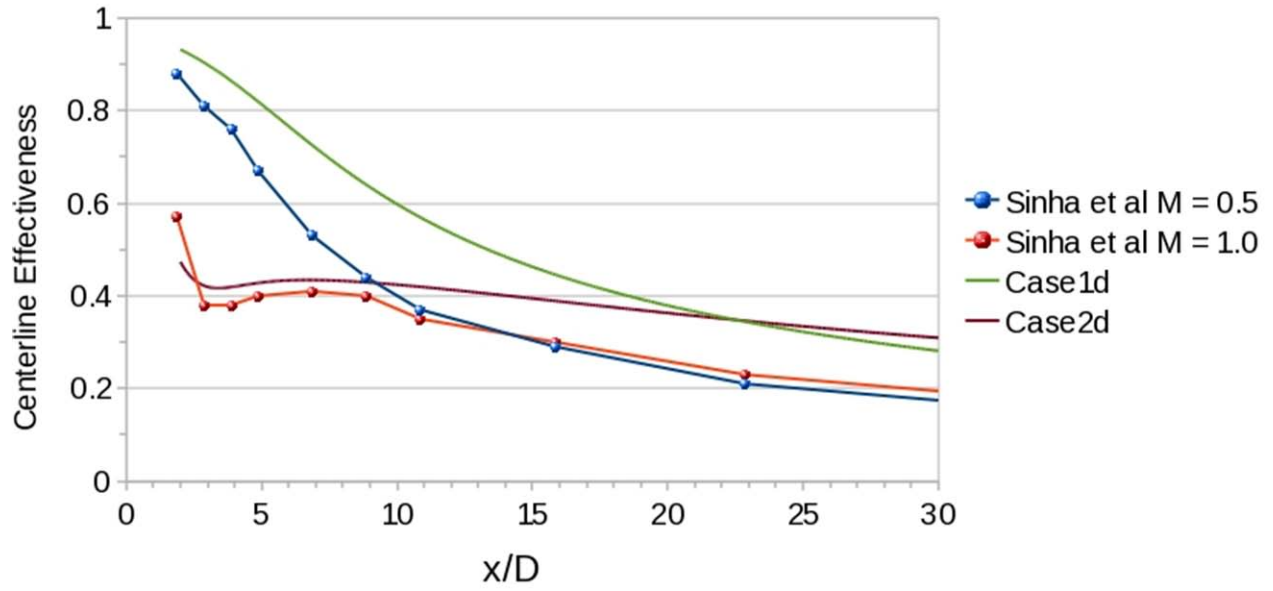
Figure 13.—Centerline effectiveness comparison for *L*/*D* = 1.75 at *I* = 0.125 versus 0.5.
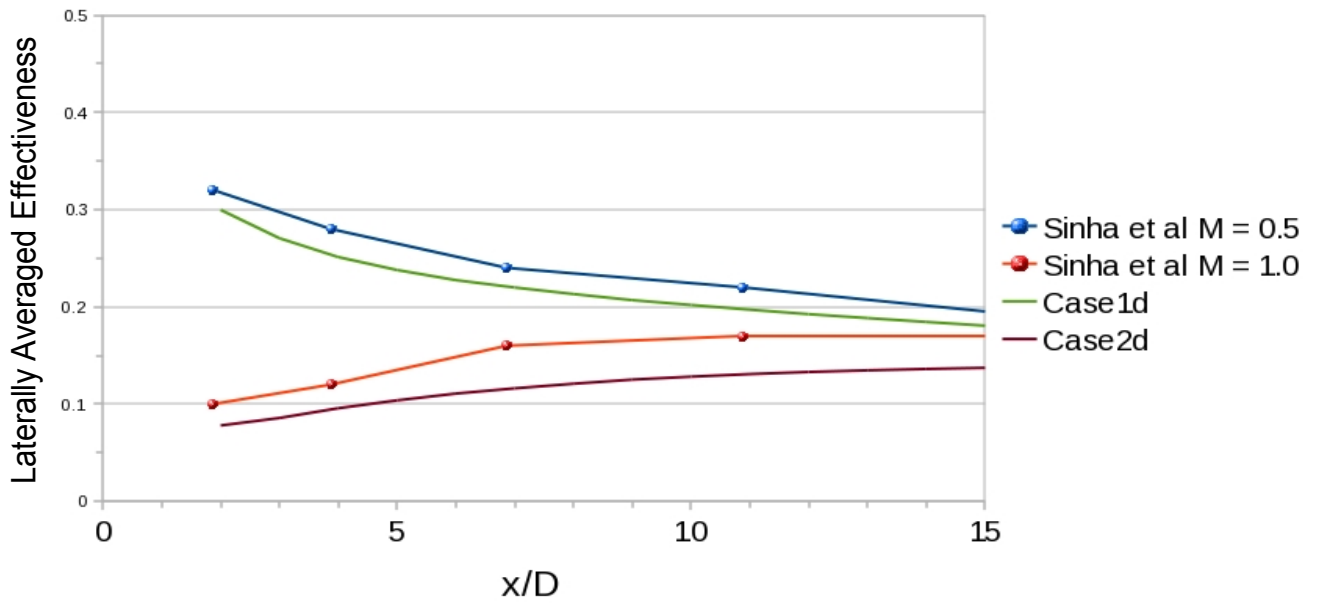

Figure 14.—Laterally averaged effectiveness comparison for *L*/*D* = 1.75 at *I* = 0.125 versus 0.5.
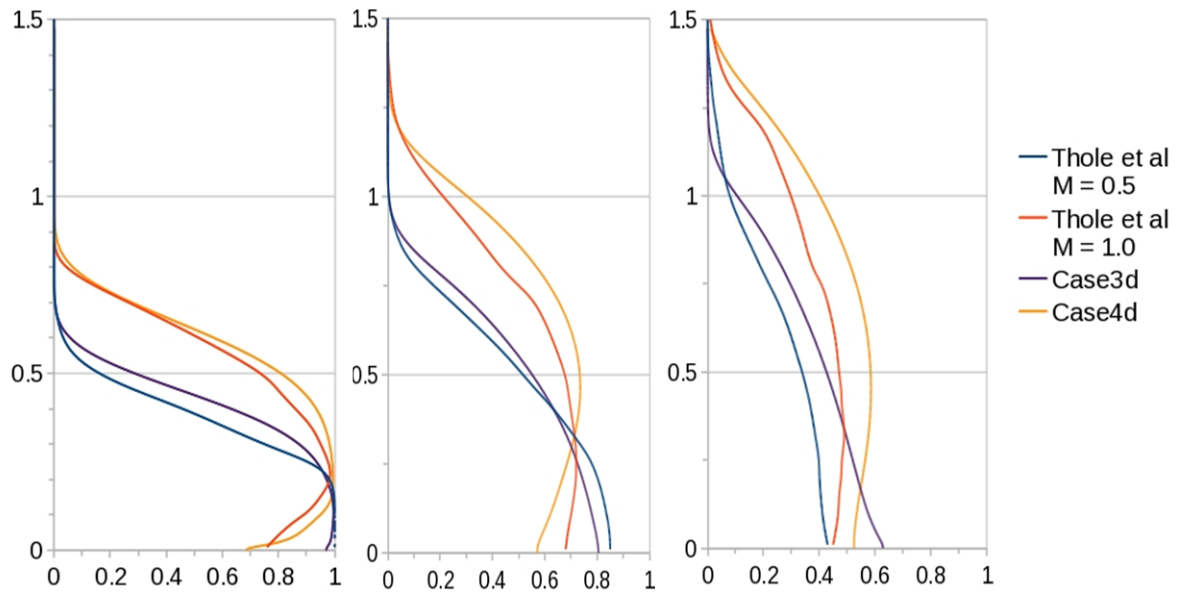
Figure 15.—Wall normal nondimensional temperature profiles for *L/D* = 3.5 at *I* = 0.125 versus 0.5.

Cases 3 and 4, with longer holes corresponding to the experiments of Thole et al. (Ref. 2), present another chance to investigate the effects of momentum ratio. Wall normal temperature profiles are presented in Figure 15. At both momentum ratios, the numerical solution tends to slightly over-predict the jet trajectory. Despite the higher mass flux rate, the higher momentum jet does not show higher jet core dimensionless temperatures than the lower momentum jet, with the slight exception of the experimental results at the further downstream point. This is perhaps due to increased entrainment of hot crossflow fluid into the jet of higher momentum balancing out the higher mass flow rate of coolant. The higher momentum jet does eventually overcome this and overtake the low momentum jet further downstream, as shown in previous results.

Length-to-Diameter Ratio Effects

Besides varying the momentum ratio, the scope of the current study also allows for a brief discussion of length-to-diameter ratio. Cases 1 and 2 correspond to the shorter hole lengths of Sinha et al. (*L/D* = 1.75), whereas Cases 3 and 4 have longer hole lengths, those of Thole et al. (*L/D* = 3.5). Hole length effects can be compared at low momentum ratios between Cases 1 and 3 and high momentum ratios between Cases 2 and 4.

Shorter holes give the coolant flow less time to develop inside the tube before injection into the crossflow. Due to the inclination angle of the jet, the coolant flowing into the hole from the plenum separates from the trailing edge of the hole inlet, unable to complete the 145° turning angle. Figure 16 shows this separation region for the higher momentum ratio case. This separation is not mirrored on the leading edge side of the coolant hole. This jetting effect produces higher velocities toward the leading edge and lower velocities in the trailing edge region, as shown in Figure 17. If the hole is long enough, the jetting effect attenuates and has little effect on the injection velocity profile. A shorter hole length will not provide the means for the jet to develop as such inside the hole. The hole exit profile, then, yields higher velocities at the leading edge. This can be seen as a higher effective inclination angle at the injection; the flow enters the hole from the plenum traveling roughly normal to the crossflow and the hole is not long enough to completely turn the coolant hole before injection. The higher effective inclination leads to lower effectiveness values, as discussed by (Refs. 11 and 12).
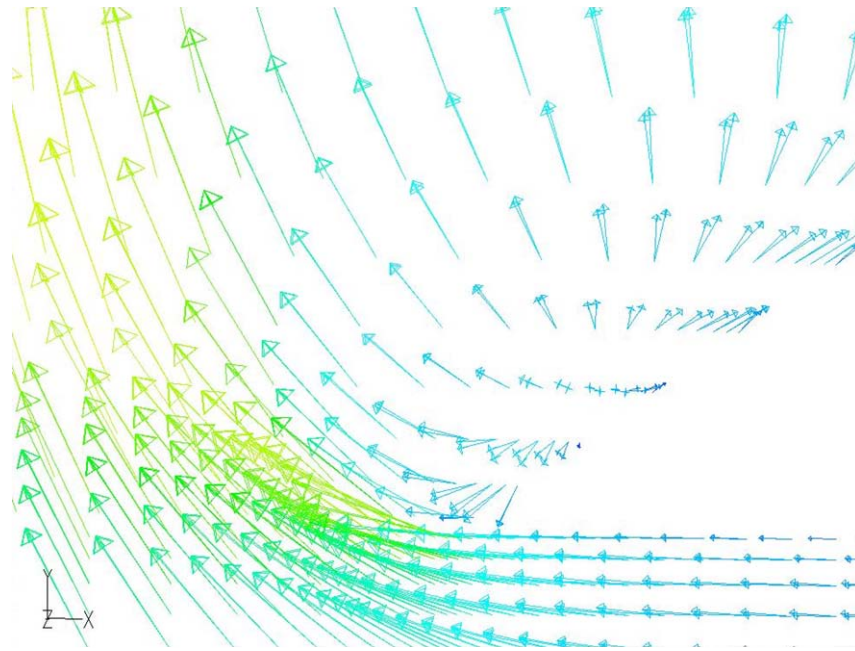
Figure 16.—Velocity vectors, colored by velocity magnitude, showing flow separation at the trailing edge of the coolant hole inlet at I = 0.5.
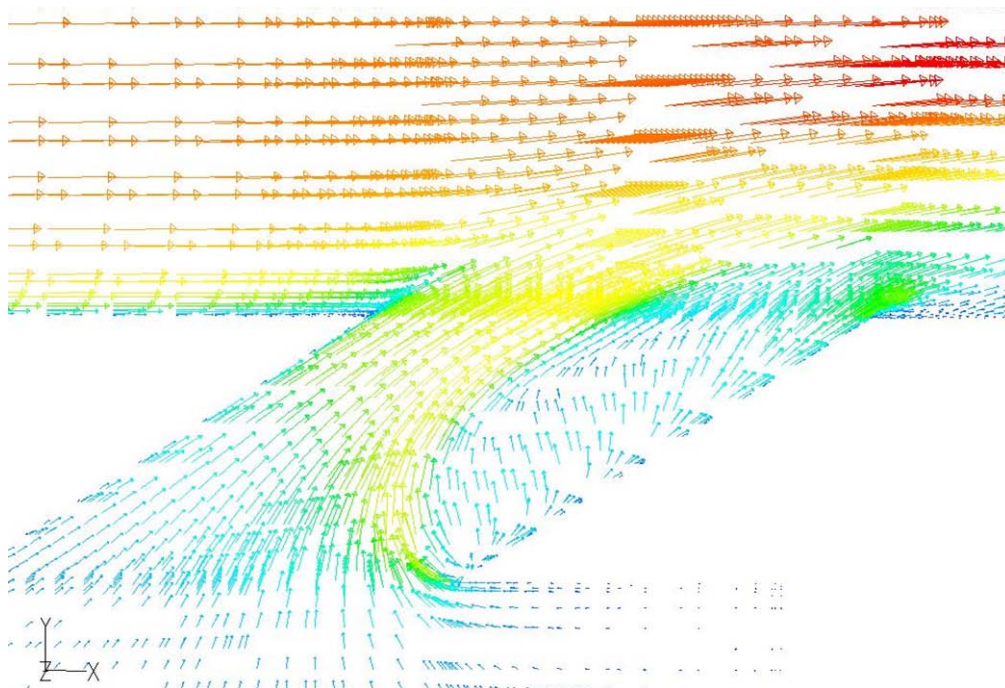

Figure 17.—Velocity vectors, colored by velocity magnitude, showing the jetting effect of the coolant inside the short hole (L/D = 1.75) at I = 0.5.

Figures 18 and 19 compare centerline and laterally-averaged effectiveness values downstream of the low momentum jets. The two hole lengths provide the same effectiveness curve. The effects of hole length is thus negligible at low momentum ratios from the viewpoint of these simulations. The coolant flow moves slowly enough that the hole quickly turns the coolant flow and there is not a significant difference between a hole of length 1.75 diameters and one twice as long. The flow at the exit of the 1.75 diameter hole may not be fully developed in the strict sense, but it is developed enough such that adding additional length to the hole does not significantly change the downstream effectiveness of the jet.
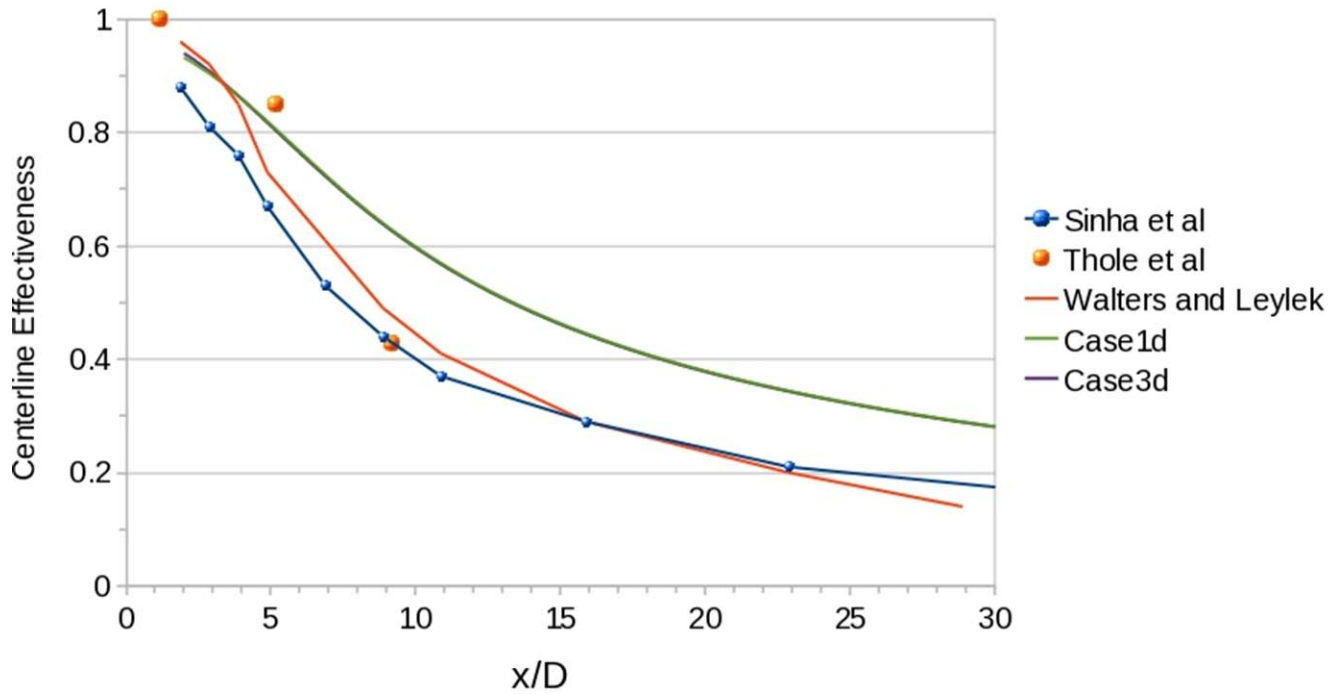

Figure 18.—Centerline effectiveness for I = 0.125 at L/D = 1.75 versus 3.5.
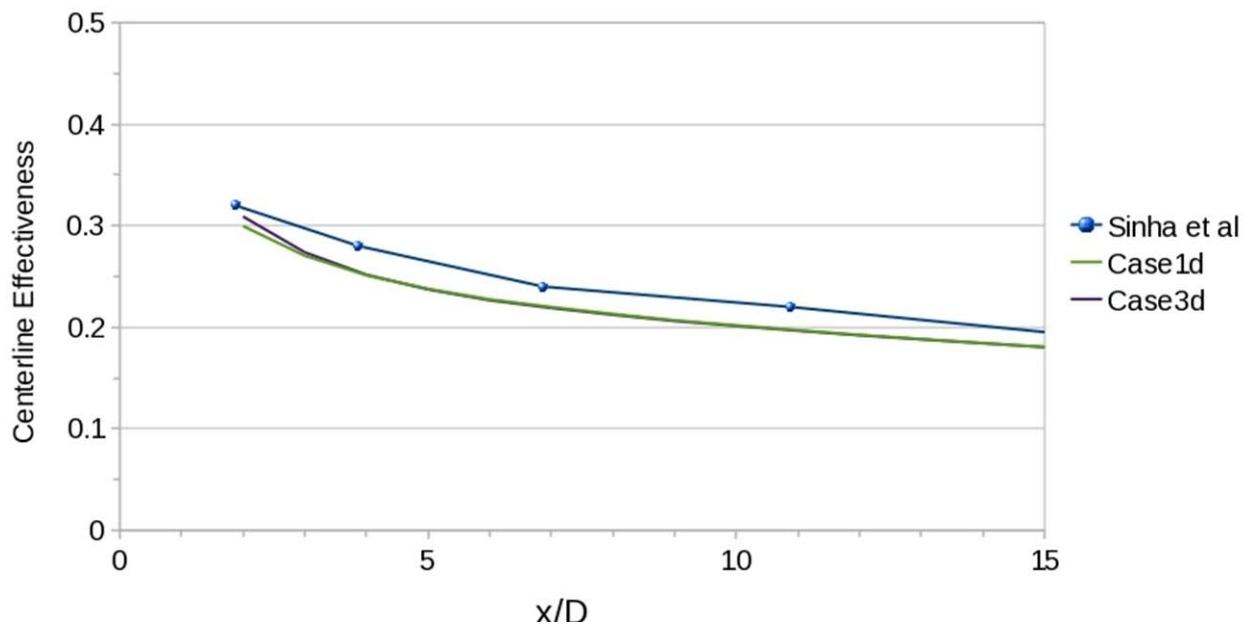

Figure 19.—Laterally Averaged effectiveness for I = 0.125 at L/D = 1.75 versus 3.5.

For the same two cases, Figure 20 shows wall normal temperature profiles at the selected downstream locations. Again, the change in the length of the hole results in no distinguishable difference in the temperature profiles.

When the momentum of the jet is increased, however, length to diameter ratio plays a larger role. Figures 21 and 22 show the effectiveness curves for the higher momentum jet ($I = 0.5$). There is now a clear difference in the effectiveness of the jet. As suspected by the above analysis, the longer hole leads to higher effectiveness values. The matching of laterally-averaged effectiveness between Case 4 and the Sinha et al. results is mere coincidence. The two results are from two different holes lengths. The proper comparison with Sinha et al. is Case 2. The inclusion of Thole et al. results in these curves is achieved by taking the asymptotic values from the wall normal profiles and plotting the three points to get a rough feel for the effectiveness predicted by those experiments.
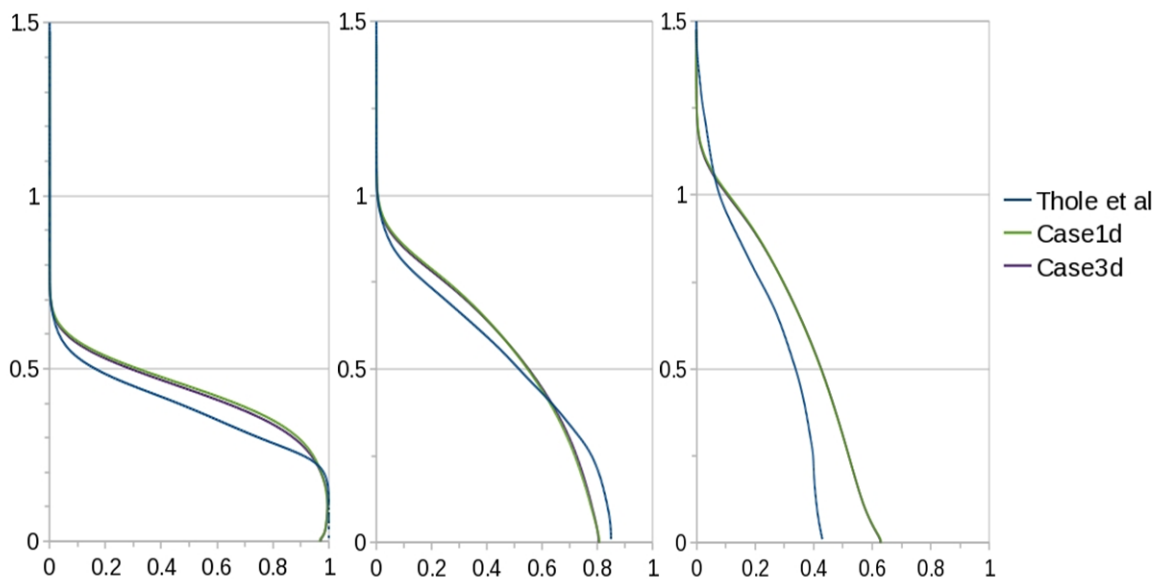
Figure 20.—Wall normal dimensionless temperature profiles for *I* = 0.125 at *L/D* = 1.75 versus 3.5.
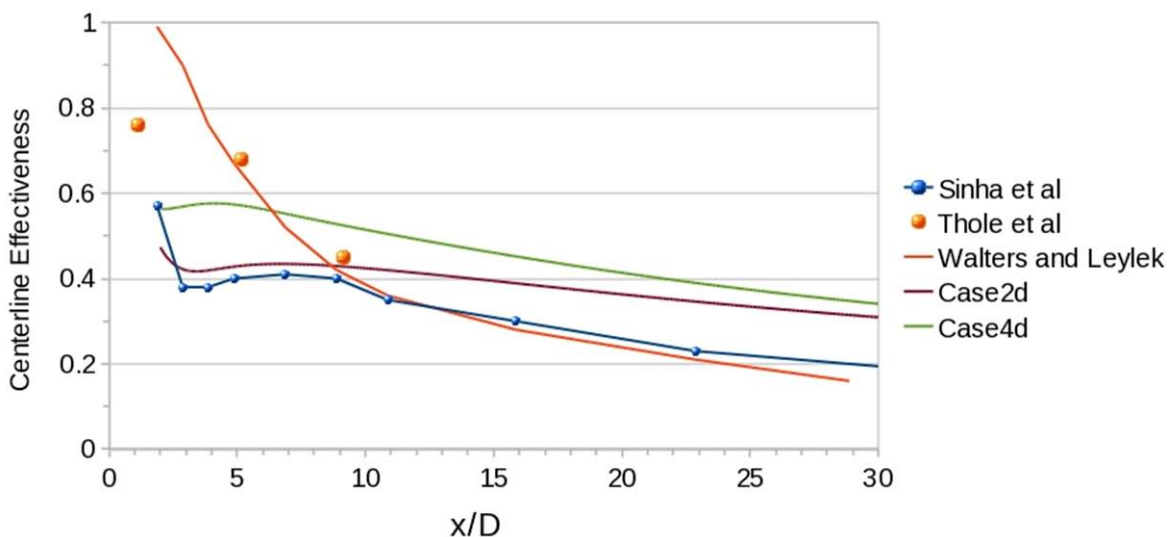
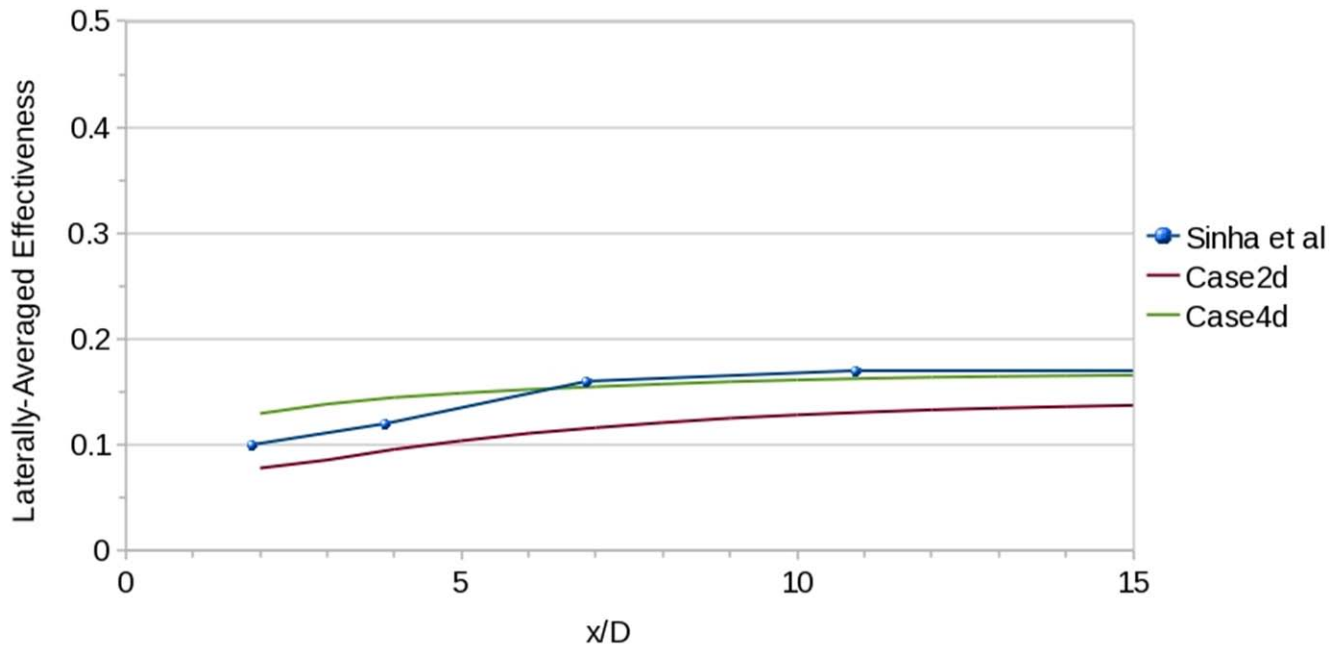Figure 21.—Centerline effectiveness trends for *I* = 0.5 at *L/D* = 1.75 versus 3.5.

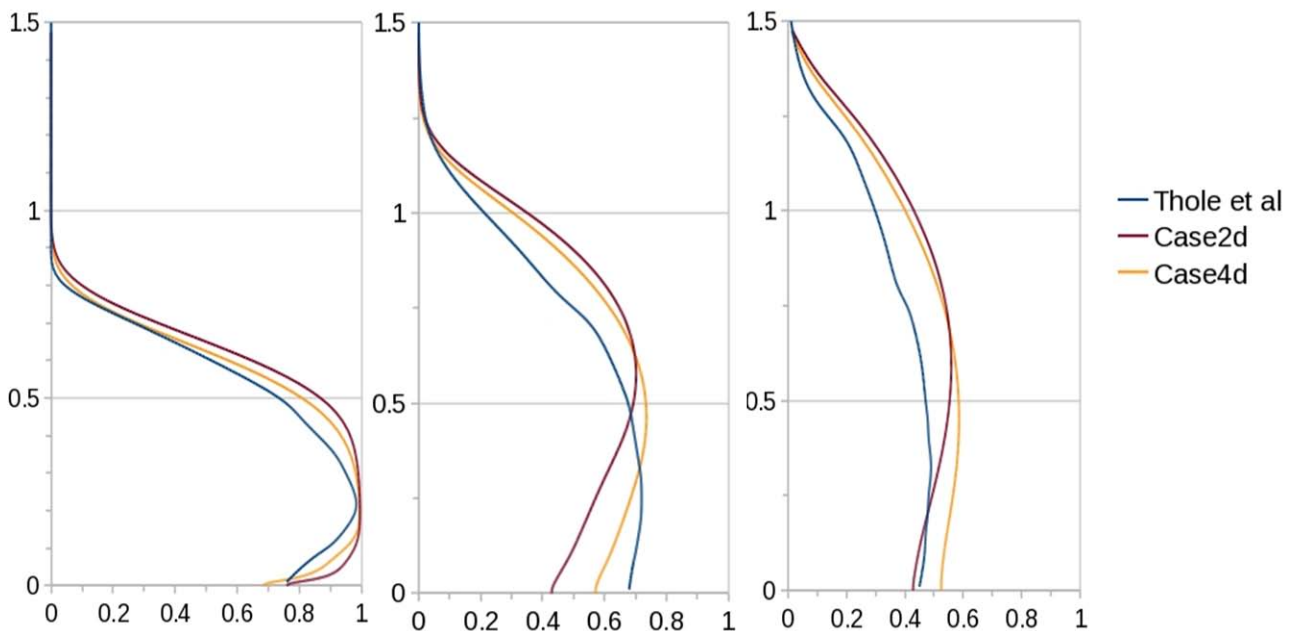Figure 22.—Laterally averaged effectiveness trends for I = 0.5 at L/D = 1.75 versus 3.5.

Figure 23.—Wall normal dimensionless temperature profiles for I = 0.5 at L/D = 1.75 versus 3.5.

This situation is further confirmed in Figure 23, where the wall normal temperature profiles are compared. The proper comparison with experimental data is Case 4. The shorter hole results show a minimum temperature (maximum non-dimensional temperature) at higher wall normal distances than the longer hole results. This indicates a higher trajectory of the coolant jet, as expected.

Conclusions

1. The domain of Walters and Leylek (Ref. 13), which is typical of RANS film cooling simulations, can be dramatically reduced in both the wall normal and upstream directions. The reduction in upstream crossflow length can be safely compensated for by the application of a 1/7 law boundary layer profile with appropriate thickness. The current case showed a 60 percent reduction in cell count with these considerations.

2. The grid refinement in the area near the trailing edge of the hole exit is crucial to the prediction of high momentum coolant jets. The RANS equations (with k-ε turbulence model) have trouble predicting the nature of recirculation in the under-side of the detached jet without ample grid points clustered near the lip. This restriction does not lead to a dramatic increase in cell count if balanced by the view that a coarser grid can be used in the crossflow. In all, a grid count under 200,000 produced results indistinguishable from the finest grid used in this study.

3. The errant nature of the k-ε model's isotropic assumption cannot be corrected by grid refinement. The universal under-prediction of lateral spreading, manifested in over-prediction of centerline effectiveness and wall normal contours in conjunction with under-prediction of laterally-averaged effectiveness, is an artifact of the turbulence model and not of discretization error.

4. Experimental trends with respect to momentum ratio and length-to-diameter ratio can be matched well with the RANS results. Higher momentum jets and shorter holes diminish the film cooling effectiveness by increasing the trajectory of the jet above the cooled surface.

5. The results of this study serve as further motivation for the use of LES in attempting to more accurately resolve the behavior of the film cooling jet. The observations of this study serve as a guide to the development of an LES film cooling approach for obtaining time-accurate solutions while resolving the larger scales of turbulence.

References

1. Sinha, A.K., Bogard, D.G., and Crawford, M.E., 1991, "Film Cooling Effectiveness Downstream of a Single Row of Holes With Variable Density Ratio," ASME Journal of Turbomachinery, 113, pp. 442–449.

2. Thole, K., Sinha, A., Bogard, D.G., and Crawford, M.E., 1992, "Mean Temperature Measurements of Jets With a Crossflow for Gas Turbine Film Cooling Application," Rotating Machinery Transport Phenomena, J.H. Kim and W.J. Yang, eds., Hemisphere Pub. Corp., New York.

3. Goldstein, R.J., Eckert, E.R.G., and Ramsey, J.W., 1968, "Film Cooling with Injection Through Holes: Adiabatic Wall Temperatures Downstream of a Circular Hole," ASME Journal of Engineering for Power, 90, pp. 384–395.

4. Goldstein, R.J., Eckert, E.R.G., Eriksen, V.L., and Ramsey, J.W., 1970, "Film Cooling Following Injection Through Inclined Circular Tubes," Israel Journal of Technology, 8, pp. 145–154.

5. Eriksen, V.L., and Goldstein, R.J., 1974, "Heat Transfer and Film Cooling Following Injection Through Inclined Circular Tubes," ASME Journal of Heat Transfer, 96, pp. 239–245.

6. Goldstein, R.J., Eckert, E.R.G., and Burggraf, F., 1974, "Effects of Hole Geometry and Density on Three-Dimensional Film Cooling," International Journal of Heat and Mass Transfer, 17, pp. 595–607.

7. Pedersen, D.R., Eckert, E.R.G., and Goldstein, R.J., 1977, "Film Cooling with Large Density Differences Between the Mainstream and the Secondary Fluid Measured by the Heat-Mass Transfer Analogy," ASME Journal of Heat Transfer, 99, pp. 620–627.

8. Foster, N.W., and Lampard, D., 1980, "The Flow and Film Cooling Effectiveness Following Injection Through a Row of Holes," ASME Journal of Engineering and Power, 102, pp. 584–588.

9. Pietrzyk, J.R., Bogard, D.G., and Crawford, M.E., 1989, "Hydrodynamic Measurements of Jets in Crossflow for Gas Turbine Film Cooling Applications," ASME Journal of Turbomachinery, 111, pp. 139–145.

10. Pietrzyk, J.R., Bogard, D.G., and Crawford, M.E., 1990, "Effects of Density Ratio on the Hydrodynamics of Film Cooling," ASME Journal of Turbomachinery, 112, pp. 57–62.
11. Burd, S.W., Kaszeta, R.W., and Simon, T.W., 1996, "Measurements in Film Cooling Flows: Hole L/D and Turbulence Intensity Effects," ASME Journal of Turbomachinery, 120, pp. 791–798.
12. Lutum, E. and Johnson, B.V., 1999, "Influence of Hole Length to Diameter Ratio on Film Cooling With Cylindrical Holes," ASME Journal of Turbomachinery, 121, pp. 233–242.
13. Walters, D.K., and Leylek, J.H., 2000, "A Detailed Analysis of Film-Cooling Physics: Part I – Streamwise Injection With Cylindrical Holes," ASME Journal of Turbomachinery, 122, pp. 102–112.
14. Azzi, A., and Lakehal, D., 2002, "Perspectives in Modeling Film Cooling of Turbine Blades by Transcending Conventional Two-Equation Turbulence Models," ASME Journal of Turbomachinery, 124, pp. 472–484.
15. Lakehal, D., 2002, "Near-Wall Modeling of Turbulent Convective Heat Transport in Film Cooling of Turbine Blades With the Aid of Direct Numerical Simulation Data," ASME Journal of Turbomachinery, 124, pp. 485–498.
16. Acharya, S., Tyagi, M., and Hoda, A., 2001, "Flow and Heat Transfer Predictions for Film Cooling," Heat transfer in gas turbine systems, Ann. N.Y. Acad. Sci., 934, pp. 110–125.
17. Tyagi, M., and Acharya, S., 2003, "Large Eddy Simulation of Film Cooling Flow From an Inclined Cylindrical Jet," J. Fluid Mech, 125, pp. 734–742.
18. Peet, Y.V., and Lele, S.K., 2008, "Near Field of Film Cooling Jet Issued Into a Flat Plate Boundary Layer: LES Study," GT2008-50420, Proceedings of ASME Turbo Expo 2008, Berlin, Germany.
19. Leedom, D.H., and Acharya, S., 2008, "Large Eddy Simulations of Film Cooling Flow Fields From Cylindrical and Shaped Holes," Proceedings of ASME Turbo Expo 2008, Berlin, Germany, GT2008-51009.
20. Renze, P., Schroder, W., Meinke, M., 2008, "Large-Eddy Simulation of Film Cooling Flows at Density Gradients," International Journal of Heat and Fluid Flow, 29, pp. 18–34.
21. Renze, P., Schroder, W., and Meinke, M., 2008, "Large-Eddy Simulation of Film Cooling Flow Ejected in a Shallow Cavity," Proceedings of the ASME Turbo Expo 2008, Berlin, Germany, GT2008-50120.
22. Rozati, A., and Tafti, D.K., 2008, "Large Eddy Simulations of Leading Edge Film Cooling: Analysis of Flow Structures, Effectiveness, and Heat Transfer Coefficient," International Journal of Heat and Fluid Flow, 29, pp. 1–17.
23. Gambit, 2008, "Gambit Version 2.3.16," USA, ANSYS Inc.
24. Fluent, 2008, "Fluent Version 6.3.26," USA, ANSYS Inc.

1. REPORT DATE (DD-MM-YYYY) 01-05-2011	2. REPORT TYPE Technical Memorandum	3. DATES COVERED (From - To)
4. TITLE AND SUBTITLE Reynolds-Averaged Navier-Stokes Solutions to Flat Plate Film Cooling Scenarios		**5a. CONTRACT NUMBER** NNC09ZA01G
		5b. GRANT NUMBER
		5c. PROGRAM ELEMENT NUMBER
6. AUTHOR(S) Johnson, Perry, L.; Shyam, Vikram; Hah, Chunill		**5d. PROJECT NUMBER**
		5e. TASK NUMBER
		5f. WORK UNIT NUMBER WBS 561581.02.08.03.21.14.03
7. PERFORMING ORGANIZATION NAME(S) AND ADDRESS(ES) National Aeronautics and Space Administration John H. Glenn Research Center at Lewis Field Cleveland, Ohio 44135-3191		**8. PERFORMING ORGANIZATION REPORT NUMBER** E-17690
9. SPONSORING/MONITORING AGENCY NAME(S) AND ADDRESS(ES) National Aeronautics and Space Administration Washington, DC 20546-0001		**10. SPONSORING/MONITOR'S ACRONYM(S)** NASA
		11. SPONSORING/MONITORING REPORT NUMBER NASA/TM-2011-217025
12. DISTRIBUTION/AVAILABILITY STATEMENT Unclassified-Unlimited Subject Categories: 02, 34, and 61 Available electronically at http://www.sti.nasa.gov This publication is available from the NASA Center for AeroSpace Information, 443-757-5802		
13. SUPPLEMENTARY NOTES		

14. ABSTRACT
The predictions of several Reynolds-Averaged Navier-Stokes solutions for a baseline film cooling geometry are analyzed and compared with experimental data. The Fluent finite volume code was used to perform the computations with the realizable k-ε turbulence model. The film hole was angled at 35° to the crossflow with a Reynolds number of 17,400. Multiple length-to-diameter ratios (1.75 and 3.5) as well as momentum flux ratios (0.125 and 0.5) were simulated with various domains, boundary conditions, and grid refinements. The coolant to mainstream density ratio was maintained at 2.0 for all scenarios. Computational domain and boundary condition variations show the ability to reduce the computational cost as compared to previous studies. A number of grid refinement and coarsening variations are compared for further insights into the reduction of computational cost. Liberal refinement in the near hole region is valuable, especially for higher momentum jets that tend to lift-off and create a recirculating flow. A lack of proper refinement in the near hole region can severely diminish the accuracy of the solution, even in the far region. The effects of momentum ratio and hole length-to-diameter ratio are also discussed.

15. SUBJECT TERMS Film cooling; Turbulence model; Heat transfer					
16. SECURITY CLASSIFICATION OF:			**17. LIMITATION OF ABSTRACT**	**18. NUMBER OF PAGES**	**19a. NAME OF RESPONSIBLE PERSON** STI Help Desk (email:help@sti.nasa.gov)
a. REPORT U	**b. ABSTRACT** U	**c. THIS PAGE** U	UU	27	**19b. TELEPHONE NUMBER** (include area code) 443-757-5802

Standard Form 298 (Rev. 8-98)
Prescribed by ANSI Std. Z39-18